ACS APPLIED MATERIALS & INTERFACES

Research Article

www.acsami.org

Ultrasensitive, Stretchable Strain Sensors Based on Fragmented Carbon Nanotube Papers

Jian Zhou,*[,†] Hu Yu,[†,‡] Xuezhu Xu,[†] Fei Han,[†] and Gilles Lubineau*[,†]

[†]King Abdullah University of Science and Technology (KAUST), Physical Sciences and Engineering Division, COHMAS Laboratory, Thuwal 23955-6900, Saudi Arabia

[‡]Shanghai Jiao Tong University, School of Mechanical Engineering, State Key Laboratory of Mechanical Systems and Vibration, 800 Dongchuan Road, Minhang District, Shanghai, 200240, P.R. China

Supporting Information

ABSTRACT: The development of strain sensors featuring both ultra high sensitivity and high stretchability is still a challenge. We demonstrate that strain sensors based on fragmented single-walled carbon nanotube (SWCNT) paper embedded in poly(dimethylsiloxane) (PDMS) can sustain their sensitivity even at very high strain levels (with a gauge factor of over 10^7 at 50% strain). This record sensitivity is ascribed to the low initial electrical resistance (5−28 Ω) of the SWCNT paper and the wide change in resistance (up to 10^6 Ω) governed by the percolated network of SWCNT in the cracked region. The sensor response remains nearly unchanged after 10 000 strain cycles at 20% proving the robustness of this technology. This fragmentation based sensing system brings opportunities to engineer highly sensitive stretchable sensors.

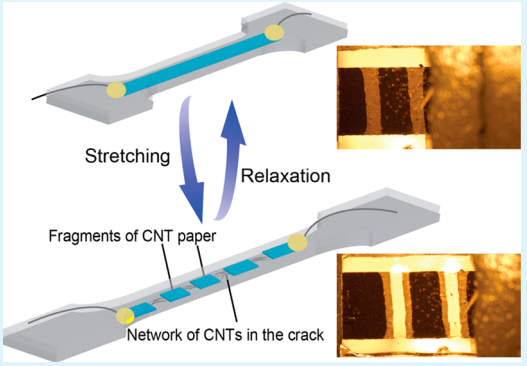

KEYWORDS: *carbon nanotube, strain sensor, crack, resistance change, sensitivity*

1. INTRODUCTION

It is now common to design flexible strain sensors using metallic nanoparticles and nanowires, carbon nanotubes (CNTs), or graphene-based materials.[1−7] However, the pursuit to design reliable strain sensors that feature high stretchability (up to 50%), high sensitivity, and durability continues. The sensitivity of a strain sensor is usually quantified by its gauge factor (GF), which is the relative change in resistance ($\Delta R/R_0$) per unit of applied strain (ε), in which ΔR and R_0 are the resistance change and the initial resistance, respectively. CNT-based strain sensors (films or fibers) have been shown to have moderate sensitivity, with the highest GF approaching 360.[3,8−12] Their sensitivity can be improved by either reducing the initial resistance or by increasing the change in resistance. This latter point is more challenging and a novel method is needed to amplify the change in resistance.

CNTs are highly conductive fillers, with volume conductivity ranging from 7×10^{-5} to 4×10^{-3} Ω cm.[13] Despite the additional resistance introduced by the CNT/CNT interface, the resistance of CNT assemblies is low enough to qualify them as candidate material for designing strain sensors when embedded in stretchable materials. Stampfer et al. demonstrated the potential of individual single-walled CNTs (SWCNTs) to sense displacement at the nanoscale, with a GF up to 2900.[14] CNTs are also used to create piezoresistive networks, in which the main sensing mechanism is the change in resistance at the CNT/CNT junctions when the network is stretched.[15] Certainly, the sensitivity of the electron tunneling mechanism plays a major role;[16] however, such studies are usually limited to small perturbations (a strain below 5%) because fibrous CNT assemblies have little elongation upon breakage.[17−19] In a previous study, we extended the stretchability to 15% by embedding SWCNT wires into elastic substrates before total mechanical and electrical breakage.[20] Here, we design a strain sensor with high sensitivity and high stretchability by introducing cracks into the SWCNT paper using the unique morphology of SWCNT networks between the crack tips as the main sensing components.

Cracks are normally considered detrimental to the overall mechanical and electrical properties of materials.[21] For example, channel crack propagation in indium−tin-oxide (ITO) coatings due to stretching or bending leads to degradation of the electrical properties of ITO-coated flexible electronics.[22,23] Similarly, microcracks appearing on conductive polymer-coated fabrics during deformation results in variation of electrical resistance.[24] However, if these cracks can be controlled, they also have the potential for use in mechanical sensing applications.[2,7,25] Strain sensors made of cracked silver nanoparticle thin film coated on PDMS substrates can be stretched to 20% with GF = 7. This change in resistance is attributed to the opening and closing of microcracks.[26] Ultrasensitive (GF > 2000) strain sensors based on the

Received: November 27, 2016
Accepted: January 17, 2017
Published: January 17, 2017

Downloaded by KING ABDULLAH UNIV SCI TECHLGY at 06:36:10:707 on May 28, 2019
from https://pubs.acs.org/doi/10.1021/acsami.6b15195.

© 2017 American Chemical Society

DOI: 10.1021/acsami.6b15195
ACS Appl. Mater. Interfaces 2017, 9, 4835−4842

formation of nanocracks in a brittle platinum thin film deposited on the top of stretchable layers have been reported; however, they had only 2% stretchability. This mechanism was based on the disconnection-reconnection process of nanoscale crack junctions under strain or vibration at the nanoscale.[25,27] Alternatively, aligned CNT film can be stretched perpendicular to the direction of alignment, fracturing the films to sustain strains up to 280%.[11] However, poor transverse interparticle conductivity of aligned CNT films coupled with high initial resistance results in sensors with very low sensitivity (GF = 0.04). By generating microcracks in the thickness gradient of the CNT film, strain sensing could be greater than 100% of the strain. However, when stretched to 15%, the GF of the sensor decreased from 161 to 0.58, showing large sensitivity deviations in the range of the strain measurement.[10] Sensors made of graphite thin films with short microcracks possess high GF (maximum value of 522.6) and high stretchability (ε > 50%), whereas sensors with long microcracks show ultrahigh sensitivity (maximum value of 11 344) with limited stretchability ($\varepsilon \leq$ 50%).[28]

Here, we introduce initial fragmentation to papers made of randomly distributed SWCNTs embedded in poly(dimethylsiloxane) (PDMS) by stretching them above their crack onset strain. The entangled networks of SWCNTs bridging the fragments throughout the cracks play a key role toward enlarging the change in electrical resistance of the strip (from 5 Ω to 30 MΩ). The sensor can measure a strain up to 50%, with a GF of 10^7. This technology is robust, whereby the performance remains unchanged up to 10 000 cycles at 20% strain. We start by describing the sensing strategy that equips our sensor with ultrahigh sensitivity and high stretchability. We identify the key parameters used to create an optimized structure by initiating cracks in the SWCNT papers. Then we show the strain sensing properties as well as their sensing mechanisms. Our concept could readily be extended to other conductive nanomaterials, paving the way for developing high-performance strain sensors.

2. MATERIALS AND METHODS

2.1. Materials. SWCNTs with 2.7 wt % COOH groups were purchased from CheapTubes, Inc. at over 90 wt % purity and containing more than 5 wt % multiwalled CNTs (MWCNT). SWCNT length ranged from 5 to 30 μm and their outer diameter ranged from 1 to 2 nm. The true density of these SWCNTs was 2.1 g/cm^3. Methanesulfonic acid (CH_3SO_3H) and SYLGARD 184 PDMS were purchased from Sigma-Aldrich.

2.2. Preparation of SWCNT Ink and Paper. An environmental friendly mild organic acid, CH_3SO_3H, was used to disperse SWCNTs to increase the safety of handling the material (compare with superacid like chlorosulfonic acid).[20] Note that if the CNT concentration was too high, alignment of the CNT could be observed and the result was a semicrystalline suspension.[36,37] Even if the acid used here is different, we prefer to work with a low concentration. The 0.5 wt % SWCNT dope was prepared by adding 0.2 g of SWCNTs into 40 g of CH_3SO_3H, sealed in a glass bottle, stirred for 5 min, and bath sonicated using a Brason 8510 sonicator (250 W) (Thomas Scientific) for 60 min. The mixture was then stirred for 12 h at 500 rpm. Different weights of 0.5% SWCNT/CH_3SO_3H dispersion were vacuum filtrated through a ceramic filtration membrane (pore size, 20 nm; Whatman). Any remaining CH_3SO_3H was removed from the sample by washing it with 200 mL of water. The thickness of 0.16, 0.31, 0.62, 0.94, 1.25, and 1.56 g cm^{-2} SWCNT paper were 15, 30, 45, 55, 70, and 90 μm, respectively. The freestanding SWCNT paper was peeled away from the filter and cut into 30 × 3 mm^2 strips for producing the strain sensors. Detailed sample information is listed in Table S1.

2.3. Preparation of the SWCNT Paper-Based Strain Sensor. A first layer of 5.3 g of PDMS (the ratio of base to curing agent was 10:1) was poured onto a 10 × 10 cm^2 Petri dish and cured at 70 °C for 12 min to obtain a sticky substrate. The strips of SWCNT paper were transferred onto the 0.5 mm-thick sticky PDMS substrates; copper wires were connected to the SWCNT paper strips by silver epoxy. Next, a second layer of PDMS of equal weight was poured onto the sample and cured at 70 °C for 2 h to fully encapsulate the SWCNT paper. The samples were cut with a standard dog-bone-shaped specimen die (ISO 527-2, Figure S2). Finally the specimen was stretched to initiate fragmentation of the SWCNT paper under a 50% strain and then relaxed to 0% strain using a 5944 Instron universal testing machine (Figure S3).

2.4. Fabrication Processes of the Electronic Fabric Integrated with Strain Sensors. First, a stretchable fabric mat was chosen as the support substrate. The first layer PDMS was casted and cured on the fabric in an area of 20 cm × 20 cm. In total, 84 strips of SWCNT paper were transferred onto the cured PDMS substrate with strain sensor units array of 6 × 6; copper wires were connected to the SWCNT paper strips by silver epoxy (the average distance between each set of electrodes is 2 cm). A second layer of PDMS of equal weight was poured onto the sample and cured at 70 °C to fully encapsulate the SWCNT paper. Finally, each SWCNT paper strip embedded in PDMS was stretched to initiate 2 to 3 cracks. The resistance data of all sensors on the fabric were collected before and after muscle stretching.

2.5. Characterizations. Scanning electron microscopy (SEM) on SWCNT paper was performed using a Quanta 3D (FEI Company). The mechanical behavior of the SWCNT paper was measured by a 5944 Instron universal testing machine at a strain rate of 0.4 mm min^{-1} by a 5-N load cell. Strips of 20 × 3 mm^2 SWCNT paper were prepared and fixed on a paper card. The tensile strength, Young's modulus, and elongation were calculated, and the values were collected from at least 10 tests for each formulation. The setup for electromechanical testing of the specimen is illustrated in Figure S3. The reversible motion (stretching/relaxing) of the sample was controlled by a 5944 Instron machine. Sliding of the sample during stretching was possible. To avoid this, we first clamped two metal plates onto the Instron machine (Figure S3). Then, we glued the dog-bone-shaped specimen to these clamps with a Devcon 5 min epoxy. We allowed the specimen to dry for 1 h before testing. We glued the whole sample region except for a 4 mm gap in the center, which defined the effective length for determining the strain during the stretching. The change in electrical resistance of the specimen was monitored using a U1252B digital multimeter. Fragmentation of the SWCNT paper created cracks and voids in the PDMS. The elongation upon breakage was about 60% with SWCNT with thicknesses of 45, 55, 70, and 90 μm. We tried to maximize the number of fragmented surfaces but not to exceed the 60% limit by fixing the maximum strain applied to any sample to 50%. Generally, fragmentation was generated on each sample by loading it to 50% strain at a speed of 0.4 mm min^{-1}. Thereafter, a cyclic stretching/relaxing program was applied with a maximum strain of 30% at each cycle. The resistance data was captured every 1 s during the test. The stretching/relaxing process of the SWCNT paper in PDMS was monitored by a video camera. For EIS, the modulus of impedance, Z, and phase angle, θ, were acquired simultaneously with an Agilent E4980A Precision LCR meter in a two-probe configuration using Kelvin clips. The frequency range spanned from 20 Hz to 2 MHz with a step of 1000 Hz and a sweep current of 50 mA. To understand the electron transport mechanism in the cracked samples, we systematically investigated the change of impedance with frequency at different applied strains (0, 10, 20, 30, 40, and 50%).

3. RESULTS AND DISCUSSION

3.1. Fragmentation of SWCNT Papers. CNT papers are not typically stretchable (strain to failure is less than 5%);[17−20,29] therefore, to introduce stretchability into the papers we embedded them into a PDMS substrate. Figure 1a

DOI: 10.1021/acsami.6b15195
ACS Appl. Mater. Interfaces 2017, 9, 4835−4842

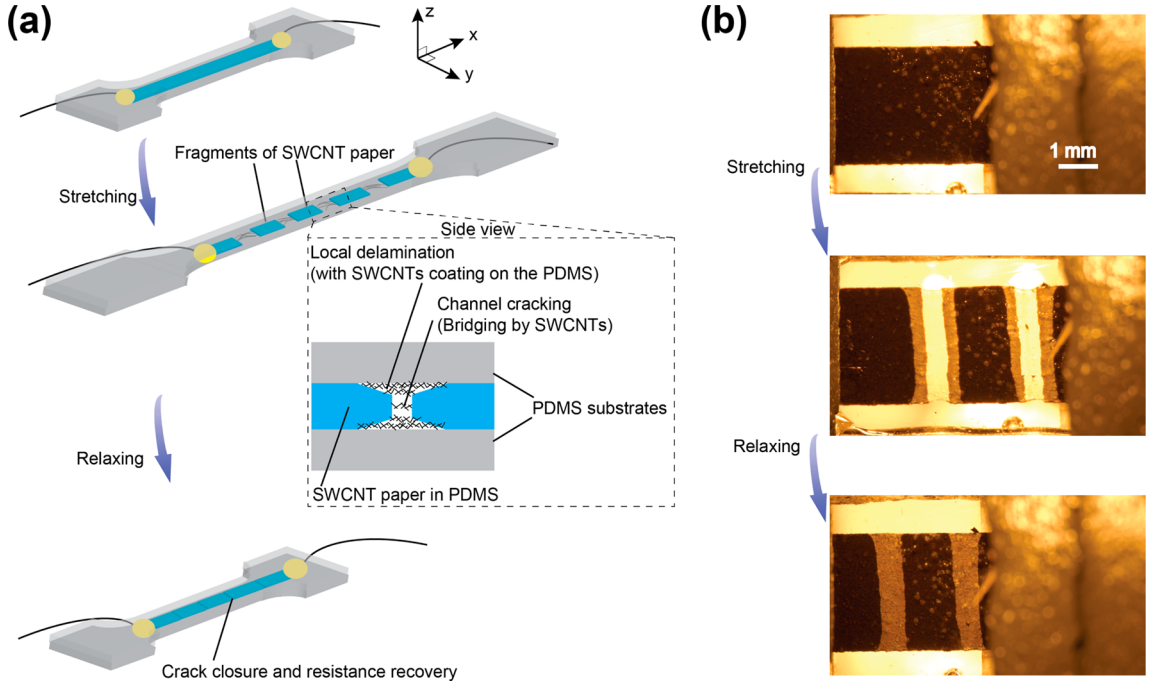

Figure 1. Proposed strategy for fragmenting SWCNT paper in PDMS to produce a high-sensitivity strain sensor. (a) Schematic presenting how SWCNT paper is fragmented in elastic substrates. Inset image shows the $x-z$ cross section of the stretched sample. Stress concentration at crack tips promotes the development of local delamination between the SWCNT paper and PDMS substrate. (b) Images of a typical 45-μm-thick SWCNT paper in PDMS being stretched to 50% strain to initiate fragmentation and then relaxed to 0% strain.

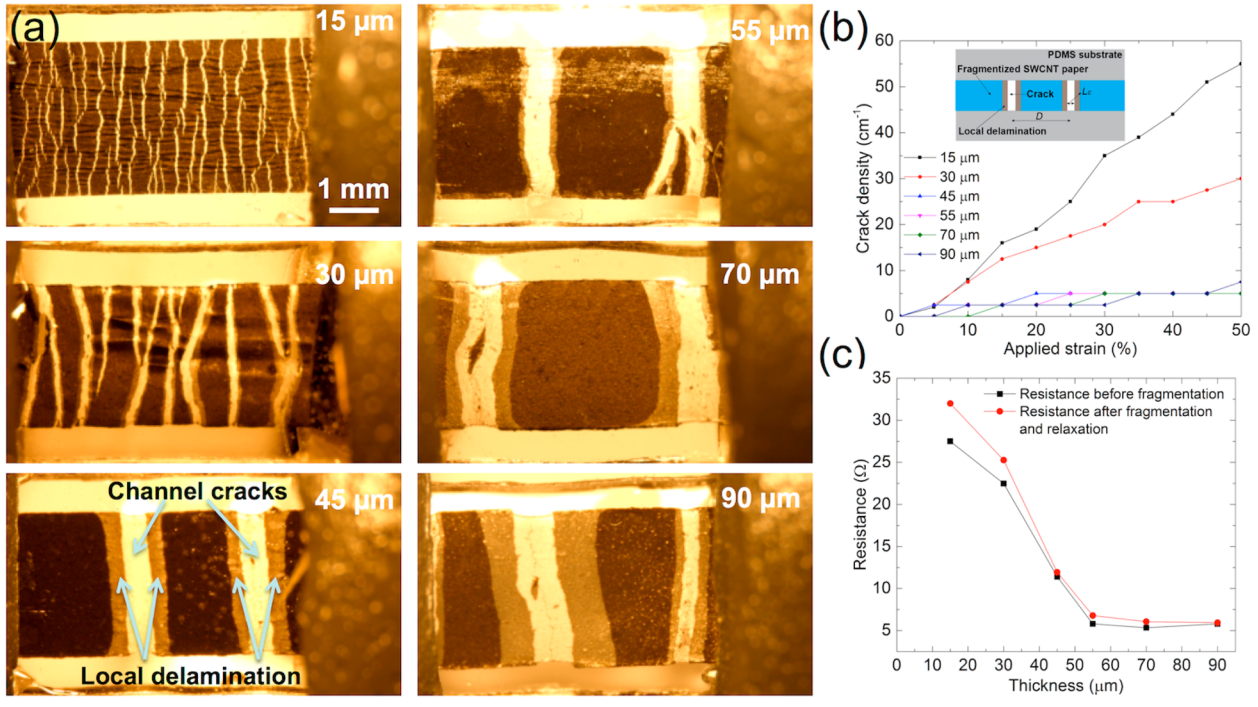

Figure 2. Thickness-controlled formation of cracks in SWCNT paper. (a) Photographs of SWCNT paper of different thicknesses embedded in elastic substrates after stretched to 50% strain. (b) Evolution of crack density with applied strain for samples of different thicknesses. We define in the inset image the average spacing between the cracks (D) and the average crack opening distance (L_c). (c) dc electrical resistance of samples without and with cracks (after relaxation).

demonstrates how a fragmented SWCNT paper sensor was fabricated and stretched (see the Materials and Methods and Supporting Information, Figures S1–S3). When this sample is stretched, the SWCNT paper fragments, while the behavior of the surrounding PDMS remains reversible (Figure 1b). When the strain is relaxed, cracks close but remain in the paper (Figure 1a,b). It is these cracks, created during the prestraining of the sample, that become central to the sensing strategy.

The cracking mechanism is typical of degradation phenomenology in laminated structures. We used a SWCNT paper with

DOI: 10.1021/acsami.6b15195
ACS Appl. Mater. Interfaces 2017, 9, 4835–4842

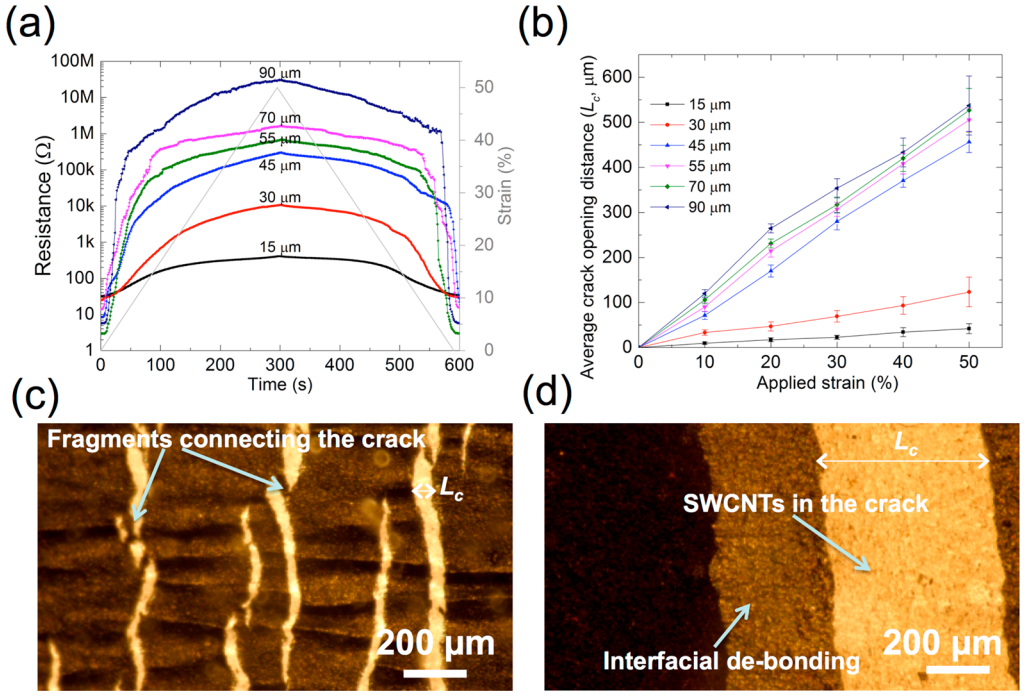

Figure 3. Fragmented SWCNT paper in PDMS as a strain sensor. (a) Resistance changes by stretching and relaxing of strain sensors. (b) Increasing average crack opening distance (L_c) with increasing applied strain. (c and d) Crack openings of the SWCNT paper in PDMS by increasing the strain to 50% for 15-μm-thick and 45-μm-thick samples, respectively.

a random, porous structure because its low strength and toughness make it easy to fragment (Figures S4 and S5). Obtaining a fragile paper required that we use a low concentration ink (0.5 wt %) with a mild acid (CH_3SO_3H) as the dispersant. When tensile load is increased, a pseudoperiodical pattern of channel cracks develops perpendicular to the principal loading direction (see Figure 2a). This is similar to the "transverse" cracking mechanism well know in laminated composites and to the channel cracking mechanisms in thin coatings, for which there are well-established micromechanical models.[23,30,31] Thus, we will not redevelop the micromechanics in entirety here, but we rely on only the results that are relevant to our study.

The first stage of the degradation is a fragmentation process that is strongly dependent on thickness. Let us define the crack density (i.e., the number of cracks per unit length about the loading direction) as $1/D$, where D is the average spacing between the cracks, as shown in the inset image of Figure 2b. Figure 2a illustrates the crack patterns at 50% strain for samples with thicknesses of 15, 30, 45, 55, 70, and 90 μm. The evolution of crack density with strain is reported for each sample on Figure 2. Two regimes can be observed: for "thin" papers (15 and 30 μm), channel cracks generally go only partially through the width and for "thick" papers (45, 55, 70, and 90 μm), very few cracks are observed, but those do run through the whole width of the sample. This is consistent with the classical micromechanics of channel cracking, where the usual distinction is done between an energy-guided regime for thin plies and a strength-guided regime for thick plies.[31]

The second stage of the degradation is the development of local delamination between the SWCNT paper and the PDMS substrate. Local delamination can be expected around crack tips because channel cracks cause severe out-of-plane stresses at the interfaces between the tips and the substrate. This process is dependent on the thickness of the ply: delamination is difficult to observe in thin paper but obvious in thick paper (45, 55, 70, and 90 μm). Furthermore, the degree of delamination depends on the balance between the energy release rate for channel cracking and the energy release rate for local delamination, the latter of which is more favorable in thick plies.

Figure 2c and Table S1 show that as paper thickness increases from 15 to 90 μm, the resistance before fragmentation (R_0) reduces from 28 to 5 Ω. For thin films (thickness below 55 μm), the resistance evolves as inverse proportional to the thickness, which indicates that the current flows through the whole thickness of the SWCNT paper. It is also a good indication that the morphology of the SWCNT packing is similar in all thin films, resulting in comparable volume resistivities. For thicker films (thickness above 55 μm), increasing the thickness does not result in further decrease in resistance. This indicates that the current only penetrates over a limited depth in the SWCNT film. The final resistance after fragmentation and relaxation is almost equal to the initial resistance (Figure 2c), indicating that after the fragmentation process, the conductive pathway can be reconnected though the flexible SWCNTs in the crack. After unloading, a very small residual increase in resistance can be observed that is coming from different source: change in morphology of the network on the crack surface and residual slippage.

3.2. Strain Sensing. The fragmented structure of SWCNT paper embedded in PDMS can now be used as high-performance strain sensors. Figure 3a presents the strain-sensing behavior of strips of the fragmented paper in PDMS when the strain ranges from 0 to 50%. The resistance of the paper increases with applied strain for all samples. Moreover, the range of relative change in resistance ($\Delta R/R_0$) can be thickness controlled. This is very important for engineering the sensitivity of the strain sensor. At 50% strain, the increase in resistance ranges from 100 Ω to 30 MΩ for 15-μm to 90-μm thick paper. We found that the resistance-changing rate at

DOI: 10.1021/acsami.6b15195
ACS Appl. Mater. Interfaces 2017, 9, 4835−4842

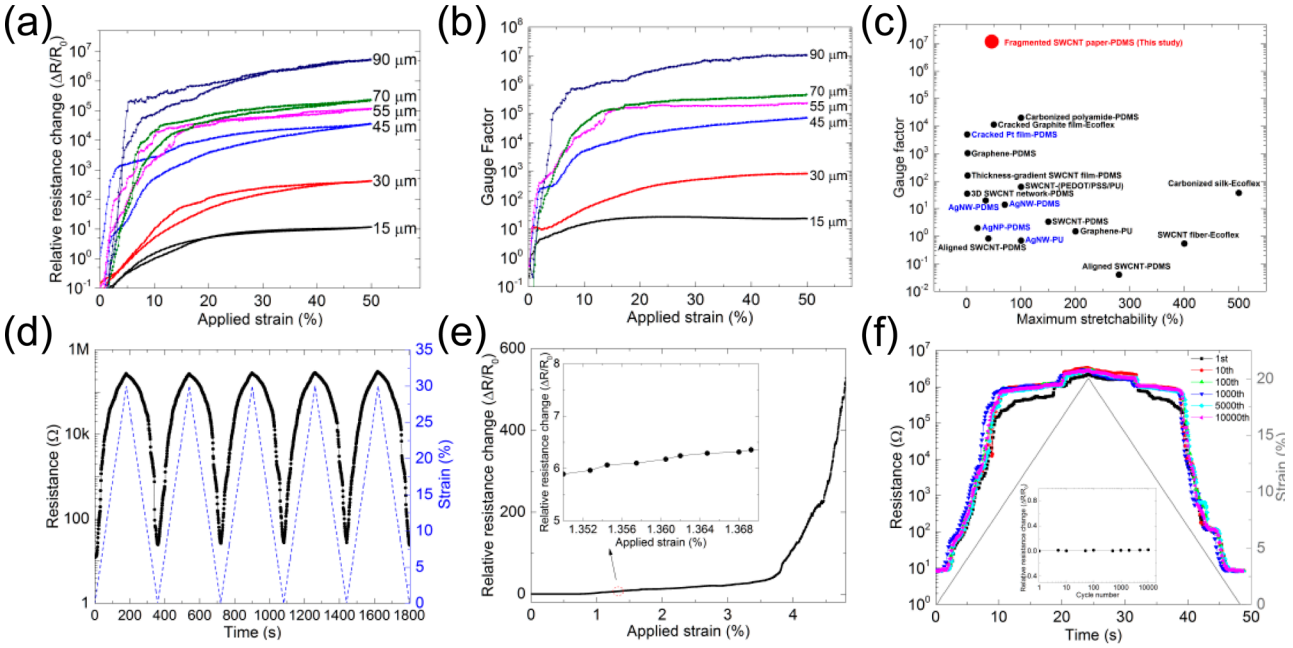

Figure 4. High sensitivity and reproducibility is achieved by the strain sensor made from fragmented SWCNT paper. (a) Relative resistance change versus applied strain of the SWCNT paper in elastic substrates during loading and unloading with a maximum applied strain of 50%. (b) GF versus applied strain for different samples. (c) GF as a function of maximum stretchability of recently reported carbon-material-based strain sensors. The GF of current study at 50% is 3 orders of magnitude higher than the best value currently reported in the literature. (d) Dynamic response of the strain sensors to five stretching/relaxing cycles at 30% with an operating rate of 0.4 mm min^{-1}. The thickness of the SWCNT paper is 90 μm. (e) Relative resistance change versus applied strain of the SWCNT. Inset shows the sensor is able to detect a strain as small as 0.002%. The stretching speed is 0.1 μm/s. (f) Resistance changes versus strain for long-term cycle test: 1, 10, 100, 1 000, 5 000, and 10 000 cycles at 0−20% strain at 2 mm min^{-1}. Inset shows that the relative resistance change after relaxation from each cycle for a total of 10 000 cycles, showing excellent long-term repeatability of the sensor. The strain sensor was also subjected to a transverse compression test while measuring its electrical resistance (Figure S7). The test was performed above the noncracked and cracked regions using a 1.25 mm-radius pressure head. Figure S7 shows the $\Delta R/R_0$ was 0 and 800 on noncracked and cracked regions, respectively, at a compression stress of 4 MPa. Thus, the cracked region of the fragmented paper is suitable for use as a highly sensitive pressure sensor.

strains lower than 10% differed from that at strains between 10% and 50%. This difference likely influences the sensing mechanism. We discuss the sensing mechanism in the following sections. The evolution of average crack opening distance, L_c, with strain is almost linear (Figure 3b), testifying to the linear elastic response of the sensor after fragmentation and relaxation. As expected, samples with larger opening distances exhibit larger resistance under strain (Figure 3c,d). For example, the resistance at a strain of 50% of 15-μm and 45-μm samples are 400 Ω and 300 kΩ, respectively. The relatively small change in resistance of thin samples is attributed mainly to small fragments connecting the cracks, ensuring residual electronic transport.

We then plot the relative change in resistance ($\Delta R/R_0$) and the GF with respect to strain in Figure 4a,b. The sizable change in resistance of 90 mm-thick SWCNT paper in PDMS enabled us to obtain a GF of 2×10^6 at $\varepsilon < 5\%$ and to reach a record GF of 10^7 at $\varepsilon = 50\%$. High sensitivities across both low and high strain levels are important to wearable applications. In comparison, conventional metal gauges have a GF around 2.0.[1,32] The GF of our sample is several orders of magnitude larger than was recently reported for stretchable strain sensors at 50% based on CNT, graphene, and silver nanomaterials (Table S3).[1−7,33] The GF value is 10^3-fold higher than the highest value of strain sensors, as shown in Figure 4c and Table S3, indicating that it could be used as an ultrasensitive strain sensor to detect subtle change in strain. We also tested the long-term performance of the sensor when exposed to cyclic stretching/relaxing. Figure 4d and Figure S6 present five cycles of a strain from 0 to 30%, in which the $\Delta R/R_0$ evolved in a very reversible and stable manner. The response time determined from Figure 4d was evaluated to be 300 ms, which is comparable with other PDMS based strain sensors.[1] The effect of channel cracks on the electrical resistance is clear at large strain but undetectable when the sample is released, indicating that the crack edges reconnect through SWCNT networks (Figure 1b).

The detection limit of the sensor was determined by applying extremely low loading speed of 0.1 μm s^{-1}. Thanks to the high sensitivity of the sensor, the relative resistance change at a strain step of 0.002% is detectable, as show from the inset in Figure 4e. The repeated opening and closing of the cracks led to reversible strain sensing with high sensitivity. Figure 4f shows that the sensor displays a very high repeatability at 1, 10, 100, 1 000, 5 000, and 10 000 cycles. After 10 000 cycles at 20% strain, the resistance of the strain sensor (SWCNT paper thickness, 90 μm) remained nearly unchanged (inset in Figure 4f).

3.3. Sensing Mechanism. Figure S8 depicts the evolution of the cracks opening in the papers with increasing applied strain to samples of two different thicknesses (15 and 45 μm). Note that stretching a precracked paper below the maximum "precracking" strain results in no additional cracks or delamination. Thus, sensing is based on existing cracks/delaminations, which were created during the precracking stage, and their development modifies electron transfer in the

DOI: 10.1021/acsami.6b15195
ACS Appl. Mater. Interfaces 2017, 9, 4835−4842

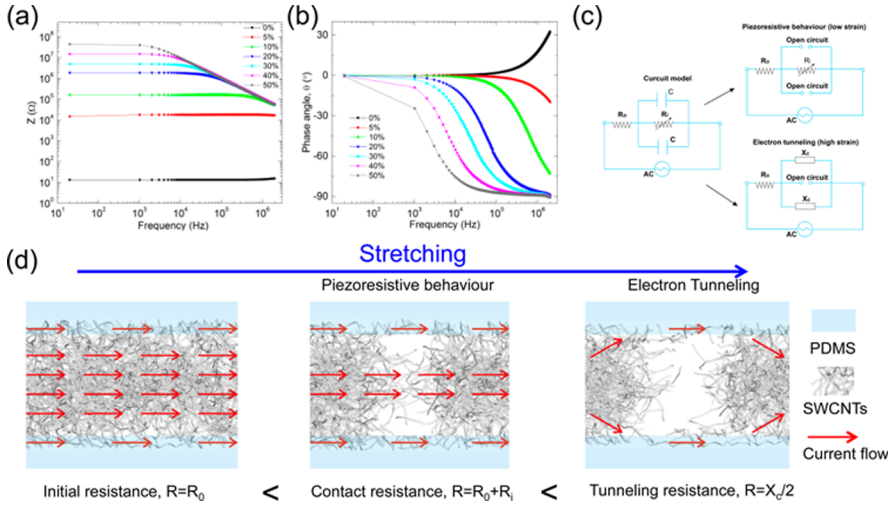

Figure 5. Sensing mechanism: (a and b) Frequency dependency of the modulus of the complex impedance (Z) and phase angle (θ), respectively. The frequency range spanned from 20 Hz to 2 MHz with a sweep current of 50 mA. (c) Equivalent circuit model of strain sensor response to applied ac stimuli. (d) Schematic images show the evolution of the SWCNT network and the current flow by increasing the applied strain in a fragmented SWCNT paper in PDMS substrate.

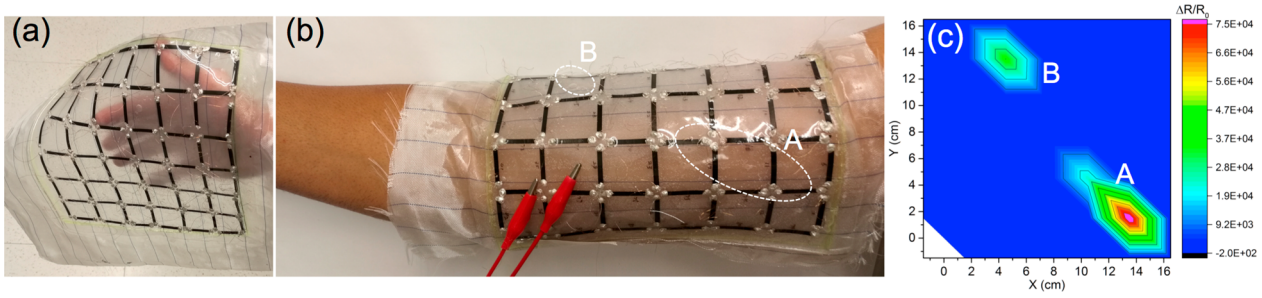

Figure 6. Demonstration of the strain sensors to a complex muscle surface. (a) Photograph of SWCNT paper-based sensors integrated on a fabric (20 cm × 20 cm), with strain sensor units array of 6 × 6. (b) The fabric with sensors was attached to bicep muscles to detect the change between relaxed and strained muscle conditions. (c) The corresponding 2D intensity profile of relative change in resistance ($\Delta R/R_0$) for each SWCNT paper sensor between relaxed and stretched muscle conditions. The areas A and B represent the location of the short (in front of the body) and long (at the side of body) head of biceps brachii muscles, respectively.

fragmented SWCNT paper. There are two ways electrical transport from one side of a crack to the other can be achieved. At low strains, direct conduction occurs between the two sides of a crack when they are in contact. Of course, when increasing the longitudinal strain, the average crack opening distance, L_C, increases, also resulting in an increase in electrical resistance (Figure 3). Both sides of a crack stay electrically connected as long as some CNTs or CNT bundles bridge them together. The cracked section of freestanding SWCNT papers we observed clearly displayed relatively aligned SWCNT bundles or single tubes that had partially pulled out from the paper. These bundles can be up to tens of micrometers in length (Figure S5) and contribute to some electrical transport even once the cracks start to open; however, at larger strains, the limited length of these bridging CNTs probably reduces their contribution to transport to negligible.

The other mechanism ensures the electrical transport up to very high strains. For example, in the case of 90-μm-thick sample, the maximum resistance is very high (20 MΩ at ε = 50%) but remains finite despite the growth of very large gaps (L_C= 500 μm). We attribute this to residual conduction at the delaminated interface. Indeed, the upper layer of PDMS peeled from the SWCNT paper was gray in color and the resistance at the interfacial layer was measured to be about 69 kΩ for a 45-μm sample (Figure S9). These results prove that our hypothesis in Figure 1a is reasonable, indicating that the PDMS precursor infiltrates the SWCNT papers to some extent during encapsulation. When delamination occurs at the PDMS/paper interface, some CNTs stay attached to the PDMS layer, resulting in a thin conductive film that continues to bridge the fragments, even at very high strains.

To identify how electron transport across the bulk and interfaces takes place, we performed a full characterization of the impedance response over a wide range of frequencies and propose an equivalent electrical circuit.[34,35] Figure 5a,b shows the frequency dependence of the modulus of the complex impedance (Z) and phase angle (θ), respectively. At low strains (ε < 10%), the impedance is nearly constant and the conduction mechanism is dominated by the resistive behavior of the SWCNT paper. Many CNT to CNT direct contacts exist and ensure macroscopic ohmic behavior. However, at higher strains, the electrical conductivity becomes considerably more frequency dependent. As strain increases, the CNTs become increasingly separated until electron tunneling becomes the dominant mechanism of electron transport. As the fragments become increasingly disconnected, the only conduction path that remains is the CNT-covered delaminated area, where the density of CNTs is less and conduction can only proceed by

DOI: 10.1021/acsami.6b15195
ACS Appl. Mater. Interfaces 2017, 9, 4835−4842

electron tunneling. This is also consistent with the phase data (Figure 5b): at larger strains (ε > 10%), the capacitive part of the sample increases with frequency. This is because the unconnected SWCNT networks act as a capacitor instead of as a resistor.

Figure 5c shows an equivalent circuit model that captures the ac behavior of the strain sensor at different strains, devised from the results of the electrical impedance spectroscopy (EIS) shown in Figure 5a,b. In the circuit, we assumed that the initial resistance of the SWCNT paper was R_0 and that it would be remain constant during stretching. While the crack resistance, R_i, was strain variant, such that its resistance increased dramatically with strain due to the sliding of CNTs in the crack. These were considered open circuits because the current did not flow through capacitance in the circuit at low strain levels. When the crack resistance approached infinity, the current flowed through the capacitance due to the electron tunneling effect, as it allows greater charge movement, ultimately reducing the overall capacitance of the thin paper.

3.4. Sensing Application. To demonstrate the sensing capabilities of our sensors on complex surfaces, an electronic fabric (20 cm × 20 cm) with 6 × 6 sensor units array was fabricated (Figure 6a). The electronic fabric was adhered to bicep muscles to detect the change between relaxed and stretched muscle conditions (Figure 6b). This complex surface of muscles represents challenges for traditional metallic gauges as it has convex and concave surface regions. The resistance of each SWCNT paper is measured before and after stretching the muscles. Mapping out the relative change in resistance ($\Delta R/R_0$) exhibits the 2D strain distribution on the electronic fabric, clearly differentiating the location of the short (A) and long (B) head of the biceps brachii muscles (Figure 6c). This demonstration highlights the potential of our sensors for characterizing tiny muscle movement with complex surfaces.

4. CONCLUSIONS

In summary, we have demonstrated that fragmented SWCNT paper in PDMS functioned as a ultrasensitive and stretchable strain sensor. Our experiments suggest a pathway toward the formation of fragmented SWCNT paper sensors with a record high GF of 10^7 at a strain of 50%. The SWCNT network in the crack plays a key role toward enlarging the range of resistance change to 10^6. The performance of such strain sensors could be tuned by changing the thickness of the SWCNT papers and the crack density. We can couple high sensitivity with medium stretchability using thick SWCNT papers or medium sensitivity with large stretchability using thin SWCNT papers in PDMS substrates. The tunability of these sensors relies mainly on the use of two very different strategies based on either intralaminar or interlaminar cracks, each of which show very different changes in conductivity when stretched. The use of fragmented carbon nanotube paper to achieve both high sensitivity and stretchability is a concept that could be readily extended to other conductive nanomaterials, paving the way for a new family of high-performance strain sensors.

■ ASSOCIATED CONTENT

Supporting Information

The Supporting Information is available free of charge on the ACS Publications website at DOI: 10.1021/acsami.6b15195.

Dispersion of SWCNT/CH_3SO_3H, sample preparation and characterization, and strain sensing (PDF)

■ AUTHOR INFORMATION

Corresponding Authors

*E-mail: jian.zhou@kaust.edu.sa.
*E-mail: gilles.lubineau@kaust.edu.sa.

ORCID

Jian Zhou: 0000-0003-0144-5901
Gilles Lubineau: 0000-0002-7370-6093

Notes

The authors declare no competing financial interest.

■ ACKNOWLEDGMENTS

We thank Dr. Erqiang Li for taking videos during measurements. Research reported in this publication was supported by baseline funding provided by King Abdullah University of Science and Technology (KAUST).

■ REFERENCES

(1) Amjadi, M.; Kyung, K.-U.; Park, I.; Sitti, M. Stretchable, Skin-mountable, and Wearable Strain Sensors and Their Potential Applications: A Review. *Adv. Funct. Mater.* **2016**, *26*, 1678−1698.

(2) Li, Z. L.; Dharap, P.; Nagarajaiah, S.; Barrera, E. V.; Kim, J. D. Carbon Nanotube Film Sensors. *Adv. Mater.* **2004**, *16*, 640−643.

(3) Lipomi, D. J.; Vosgueritchian, M.; Tee, B. C. K.; Hellstrom, S. L.; Lee, J. A.; Fox, C. H.; Bao, Z. N. Skin-like Pressure and Strain Sensors Based on Transparent Elastic Films of Carbon Nanotubes. *Nat. Nanotechnol.* **2011**, *6*, 788−792.

(4) Jeong, Y. R.; Park, H.; Jin, S. W.; Hong, S. Y.; Lee, S. S.; Ha, J. S. Highly Stretchable and Sensitive Strain Sensors Using Fragmentized Graphene Foam. *Adv. Funct. Mater.* **2015**, *25*, 4228−4236.

(5) Cheng, Y.; Wang, R.; Sun, J.; Gao, L. A Stretchable and Highly Sensitive Graphene-based Fiber for Sensing Tensile Strain, Bending, and Torsion. *Adv. Mater.* **2015**, *27*, 7365−7371.

(6) Amjadi, M.; Pichitpajongkit, A.; Lee, S.; Ryu, S.; Park, I. Highly Stretchable and Sensitive Strain Sensor Based on Silver Nanowire-Elastomer Nanocomposite. *ACS Nano* **2014**, *8*, 5154−5163.

(7) Kim, K. K.; Hong, S.; Cho, H. M.; Lee, J.; Suh, Y. D.; Ham, J.; Ko, S. H. Highly Sensitive and Stretchable Multidimensional Strain Sensor with Prestrained Anisotropic Metal Nanowire Percolation Networks. *Nano Lett.* **2015**, *15*, 5240−5247.

(8) Zhao, H. B.; Zhang, Y. Y.; Bradford, P. D.; Zhou, Q. A.; Jia, Q. X.; Yuan, F. G.; Zhu, Y. T. Carbon Nanotube Yarn Strain Sensors. *Nanotechnology* **2010**, *21*, 305502.

(9) Lekawa-Raus, A.; Kurzepa, L.; Peng, X. Y.; Koziol, K. Towards the Development of Carbon Nanotube Based Wires. *Carbon* **2014**, *68*, 597−609.

(10) Liu, Z. Y.; Qi, D. P.; Guo, P. Z.; Liu, Y.; Zhu, B. W.; Yang, H.; Liu, Y. Q.; Li, B.; Zhang, C. G.; Yu, J. C.; Liedberg, B.; Chen, X. D. Thickness-Gradient Films for High Gauge Factor Stretchable Strain Sensors. *Adv. Mater.* **2015**, *27*, 6230−6237.

(11) Yamada, T.; Hayamizu, Y.; Yamamoto, Y.; Yomogida, Y.; Izadi-Najafabadi, A.; Futaba, D. N.; Hata, K. A Stretchable Carbon Nanotube Strain Sensor for Human-motion Detection. *Nat. Nanotechnol.* **2011**, *6*, 296−301.

(12) Ryu, S.; Chou, J. B.; Lee, K.; Lee, D.; Hong, S. H.; Zhao, R.; Lee, H.; Kim, S. G. Direct Insulation-to-Conduction Transformation of Adhesive Catecholamine for Simultaneous Increases of Electrical Conductivity and Mechanical Strength of CNT Fibers. *Adv. Mater.* **2015**, *27*, 3250−3255.

(13) Ebbesen, T. W.; Lezec, H. J.; Hiura, H.; Bennett, J. W.; Ghaemi, H. F.; Thio, T. Electrical Conductivity of Individual Carbon Nanotubes. *Nature* **1996**, *382*, 54−56.

(14) Stampfer, C.; Jungen, A.; Linderman, R.; Obergfell, D.; Roth, S.; Hierold, C. Nano-electromechanical Displacement Sensing Based on Single-walled Carbon Nanotubes. *Nano Lett.* **2006**, *6*, 1449−1453.

DOI: 10.1021/acsami.6b15195
ACS Appl. Mater. Interfaces 2017, 9, 4835−4842

(15) Gong, C. K.; Liang, J. J.; Hu, W.; Niu, X. F.; Ma, S. W.; Hahn, H. T.; Pei, Q. B. A Healable, Semitransparent Silver Nanowire-Polymer Composite Conductor. *Adv. Mater.* **2013**, *25*, 4186−4191.
(16) Simmons, J. Generalized Formula for the Electric Tunnel Effect between Similar Electrodes Separated by a Thin Insulating Film. *J. Appl. Phys.* **1963**, *34*, 1793−1803.
(17) Malik, S.; Rosner, H.; Hennrich, F.; Bottcher, A.; Kappes, M. M.; Beck, T.; Auhorn, M. Failure Mechanism of Free Standing Single-walled Carbon Nanotube Thin Films under Tensile Load. *Phys. Chem. Chem. Phys.* **2004**, *6*, 3540−3544.
(18) Kumar, N. A.; Jeon, I. Y.; Sohn, G. J.; Jain, R.; Kumar, S.; Baek, J. B. Highly Conducting and Flexible Few-Walled Carbon Nanotube Thin Film. *ACS Nano* **2011**, *5*, 2324−2331.
(19) Di, J. T.; Hu, D. M.; Chen, H. Y.; Yong, Z. Z.; Chen, M. H.; Feng, Z. H.; Zhu, Y. T.; Li, Q. W. Ultrastrong, Foldable, and Highly Conductive Carbon Nanotube Film. *ACS Nano* **2012**, *6*, 5457−5464.
(20) Zhou, J.; Xu, X.; Yu, H.; Lubineau, G. Deformable and Wearable Carbon Nanotube Microwire-based Sensors for Ultrasensitive Monitoring of Strain, Pressure and Torsion. *Nanoscale* **2017**, *9*, 604−612.
(21) Zhang, J.; Liu, J. W.; Zhuang, R. C.; Mader, E.; Heinrich, G.; Gao, S. L. Single MWNT-Glass Fiber as Strain Sensor and Switch. *Adv. Mater.* **2011**, *23*, 3392−3397.
(22) Leterrier, Y.; Pinyol, A.; Rougier, L.; Waller, J. H.; Manson, J. A. E. Electrofragmentation Modeling of Conductive Coatings on Polymer Substrates. *J. Appl. Phys.* **2009**, *106* (11), 113508.
(23) Saleh, M. N.; Lubineau, G. Understanding the Mechanisms that Change the Conductivity of Damaged ITO-coated Polymeric Films: A Micro-mechanical Investigation. *Sol. Energy Mater. Sol. Cells* **2014**, *130*, 199−207.
(24) Wang, Y.; Shi, Z. X.; Fang, J. H.; Xu, H. J.; Ma, X. D.; Yin, J. Direct Exfoliation of Graphene in Methanesulfonic Acid and Facile Synthesis of Graphene/polybenzimidazole Nanocomposites. *J. Mater. Chem.* **2011**, *21*, 505−512.
(25) Kang, D.; Pikhitsa, P. V.; Choi, Y. W.; Lee, C.; Shin, S. S.; Piao, L. F.; Park, B.; Suh, K. Y.; Kim, T. I.; Choi, M. Ultrasensitive Mechanical Crack-based Sensor Inspired by the Spider Sensory System. *Nature* **2014**, *516*, 222−226.
(26) Lee, J.; Kim, S.; Lee, J.; Yang, D.; Park, B. C.; Ryu, S.; Park, I. A Stretchable Strain Sensor Based on A Metal Nanoparticle Thin Film for Human Motion Detection. *Nanoscale* **2014**, *6*, 11932−11939.
(27) Yang, T.; Li, X.; Lin, S.; Lao, J.; Shi, J.; Zhen, Z.; Li, Z.; Zhu, H. Structural Engineering of Gold Thin Films with Channel Cracks for Ultrasensitive Strain Sensing. *Mater. Horiz.* **2016**, *3*, 248−255.
(28) Amjadi, M.; Turan, M.; Clementson, C. P.; Sitti, M. Parralle Microcracks-based Ultrasensitive Highly Stretchable Strain Sensors. *ACS Appl. Mater. Interfaces* **2016**, *8*, 5618−5626.
(29) Zhang, D. L.; Ju, X.; Li, L. H.; Kang, Y.; Gong, X. L.; Li, B. J.; Zhang, S. An Efficient Multiple Healing Conductive Composite via Host-guest Inclusion. *Chem. Commun.* **2015**, *51*, 6377−6380.
(30) Arteiro, A.; Catalanotti, G.; Melro, A. R.; Linde, P.; Camanho, P. P. Micro-mechanical Analysis of the in situ Effect in Polymer Composite Laminates. *Compos Struct.* **2014**, *116*, 827−840.
(31) Arteiro, A.; Catalanotti, G.; Melro, A. R.; Linde, P.; Camanho, P. P. Micro-mechanical Analysis of the Effect of Ply Thickness on the Transverse Compressive Strength of Polymer Composites. *Composites, Part A* **2015**, *79*, 127−137.
(32) Park, J.; You, I.; Shin, S.; Jeong, U. Material Approaches to Stretchable Strain Sensors. *ChemPhysChem* **2015**, *16*, 1155−1163.
(33) Obitayo, W.; Liu, T. A Review: Carbon Nanotube-Based Piezoresistive Strain Sensors. *J. Sens.* **2012**, *2012*, 652438.
(34) Sangeeth, C. S. S.; Wan, A.; Nijhuis, C. A. Equivalent Circuits of a Self-Assembled Monolayer-Based Tunnel Junction Determined by Impedance Spectroscopy. *J. Am. Chem. Soc.* **2014**, *136*, 11134−11144.
(35) Ventura, I. A.; Zhou, J.; Lubineau, G. Investigating the Inter-Tube Conduction Mechanism in Polycarbonate Nanocomposites Prepared with Conductive Polymer-Coated Carbon Nanotubes. *Nanoscale Res. Lett.* **2015**, *10*, 485.
(36) Parra-Vasquez, A. N. G.; Behabtu, N.; Green, M. J.; Pint, C. L.; Young, C. C.; Schmidt, J.; Kesselman, E.; Goyal, A.; Ajayan, P. M.; Cohen, Y.; Talmon, Y.; Hauge, R. H.; Pasquali, M. Spontaneous Dissolution of Ultralong Single- and Multiwalled Carbon Nanotubes. *ACS Nano* **2010**, *4*, 3969−3978.
(37) Davis, V. A.; Parra-Vasquez, A. N. G.; Green, M. J.; Rai, P. K.; Behabtu, N.; Prieto, V.; Booker, R. D.; Schmidt, J.; Kesselman, E.; Zhou, W.; Fan, H.; Adams, W. W.; Hauge, R. H.; Fischer, J. E.; Cohen, Y.; Talmon, Y.; Smalley, R. E.; Pasquali, M. True Solutions of Single-walled Carbon Nanotubes for Assembly into Macroscopic Materials. *Nat. Nanotechnol.* **2009**, *4*, 830−834.

DOI: 10.1021/acsami.6b15195
ACS Appl. Mater. Interfaces 2017, 9, 4835−4842